A New, Computationally Efficient "Blech Criterion" for Immortality in General Interconnects

Mohammad Abdullah Al Shohel, Vidya A. Chhabria, and Sachin S. Sapatnekar
Department of Electrical and Computer Engineering
University of Minnesota, Minneapolis, MN 55455, USA.

Abstract—**Traditional methodologies for analyzing electromigration (EM) in VLSI circuits first filter immortal wires using Blech's criterion, and then perform detailed EM analysis on the remaining wires. However, Blech's criterion was designed for two-terminal wires and does not extend to general structures. This paper demonstrates a first-principles-based solution technique for determining the steady-state stress at all the nodes of a general interconnect structure, and develops an immortality test whose complexity is linear in the number of edges of an interconnect structure. The proposed model is applied to a variety of structures. The method is shown to match well with results from numerical solvers, to be scalable to large structures.**

I. INTRODUCTION

Electromigration (EM) aging in metal wires is caused by material transport of atoms, triggered by electron current through the wires. EM has become a major concern in electronic circuits due to the increase in current density. Previously, EM was considered a problem only in upper metal layers that carry the largest current, but with scaling, as transistors drive increasing amounts of current through narrow wires, EM hotspots have emerged through the stack.

The conventional method for EM analysis for interconnects involves a two-stage process. In the first stage, EM-immune wires are filtered out using the Blech criterion [1], which compares the product of the current density j through a wire with its length, l. This jl product is compared against a technology-specific threshold, and any wires that fall below this product are deemed immortal, while others are potentially mortal. In the second stage, wires in the latter class undergo further analysis to check whether or not the EM failure may occur during the product lifespan. Traditionally, this involves a comparison of the current density through these wires against a global limit, set by the semi-empirical Black's equation [2]; more recent approaches include [3]–[6].

However, this approach is predicated on analyses/characterizations of single-wire-segment test structures, which determine the critical jl product threshold for the Blech criterion, and the upper bound on j in Black's equation. In practice, wires typically have multiple segments with different current densities. The criterion for immortality under this scenario is quite different from the Blech criterion, and while the limitations of the criterion have been widely recognized in past work, there is no computationally simple test similar to the Blech criterion to determine immortality for general interconnects.

As opposed to the empirical Black's equation based approach, there has been an emerging thread on using physics-based analysis for EM in interconnects. Building upon past work such as [7]–[9], the work in [10] presented a canonical treatment of EM equations in a metallic interconnect, with exact solutions for a semi-infinite and finite line. This paper has formed the basis of much work since then, with techiques that attempt to obtain solutions for a single-segment lines [3], [11]. For multisegment lines, several attempts have been made to solve the general transient analysis problem [3], [4] through detailed simulations, but the key to checking for immortality is to solve the *steady-state* problem. The methods in [12], [13],
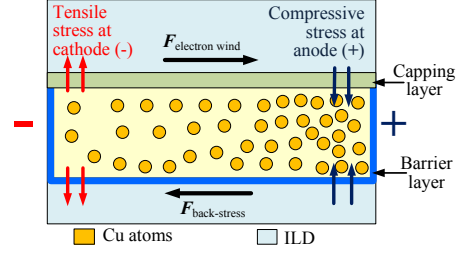
Figure 1: Cross section of a Cu wire indicating the electron wind force and back-stress force [6].

subsequently extended in [14], used a sum of jl products along wire segments: if j_i is the current density through the ith segment of length l_i, then the largest $\sum j_i l_i$ on any path in a tree was taken to be the worst-case stress: as observed in [15], this is incorrect.

In [16], a system of equations describing steady-state analysis in an interconnect tree was presented and solved. However, the structure of the difference equations was not exploited to obtain a generalizable solution. The analyses in [17], [18] solve a related problem for a simple two- or three-segment structure with a passive reservoir. The work in [19] develops analysis principles and applies them to several structures, with closed-form formulas for simple topologies. However, it does not provide a scalable algorithm for general structures.

Thus, there is no truly general, scalable formula for immortality detection to replace the Blech criterion. This work solves this problem with a linear-time algorithm for general multisegment interconnects. On comparable CPUs, our approach provides solutions to IBM PG benchmarks in a few minutes, while [19] requires over an hour.

II. BACKGROUND

Figure 1 illustrates the electromigration mechanism in a Cu dual-damascene (DD) wire. As the current flows in a metal wire, metal atoms are transported from the cathode towards the anode, in the direction of electron flow, by the momentum of the electrons. This electron wind force causes a depletion of metal atoms at the cathode, potentially resulting in void formation, leading to open circuits. In a Cu DD interconnect, the movement of migrating atoms occurs in a single metal layer, and atoms are prevented from migrating to other metal layers due to the capping or barrier layer, which acts as a blocking boundary for mass transport [20], [21]. Consequently, within a metal layer, mass depletion of atoms occurs at the cathode terminal and mass accumulation occurs at the anode terminal. A tensile stress is created near the anode, and a compressive stress near the cathode.

The concentration gradient caused by metal migration creates a tendency for atoms to diffuse back to the cathode. This force, acting against the electron wind, is proportional to the stress gradient.

A. Notation

For a general interconnect structure with multiple segments, we define the following notation. This is represented by an undirected graph $\mathcal{G}(V, E)$ with $|E|$ segments and $|V|$ nodes. The vertices
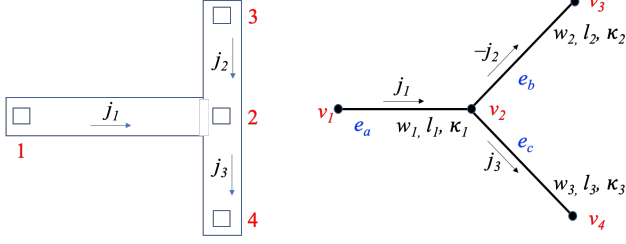
Figure 2: (a) A simple net fragment. (b) Its equivalent graph, with arrows showing the reference current direction for each edge.

$V = \{v_1, \cdots, v_{|V|}\}$ are the set of *nodes* in the structure, and edges $E = \{e_1, \cdots, e_{|E|}\}$ are the set of wire *segments*. A vertex of degree 1 is referred to as a *terminus*.

Each edge e_i is associated with a reference current direction, and has three attributes: length l_i, width w_i, and current density j_i. The sign of current density is relative to the reference direction of the edge: it is negative if the current is opposite to the reference direction. Figure 2 shows a net fragment and its graph model for a tree with four nodes and three edges: since the current direction in e_b is opposite to the reference direction, the current density is shown as $-j_2$.

Along each edge, we use a *local coordinate system* along each segment i. If the edge has a reference direction from node v_a to node v_b, we represent the position of node a as $x = 0$ and that of node b as $x = l_i$. As part of our analysis, we will compute stresses induced within the interconnect. Specifically,

- $\sigma_i(x, t)$ is the stress within wire *segment i* at time t at a location x, where $0 \leq x \leq l_i$ and $1 \leq i \leq |E|$.
- σ^k is the steady-state stress at *node v_k*, $1 \leq k \leq |V|$.

B. Stress equations for interconnect structures

A single interconnect segment injects electron current at a cathode at $x = 0$ towards an anode at $x = l_i$. The temporal evolution of EM-induced stress, $\sigma(x, t)$, in the segment is modeled as [10]:

$$\frac{\partial \sigma}{\partial t} = \frac{\partial}{\partial x}\left[\kappa\left(\frac{\partial \sigma}{\partial x} + \beta j_i\right)\right] \quad (1)$$

Here, x is the distance from the cathode; $\beta = (Z^* e\rho)/\Omega$; j_i is the current density through the wire; Z^* is the effective charge number; e is the electron charge; ρ is the resistivity; and Ω is the atomic volume for the metal (in the literature, βj_i is often denoted as G). Here, $\kappa = D_a \mathcal{B}\Omega/(kT)$, where $\mathcal{B}$ is the bulk modulus of the material, k is Boltzmann's constant, and T is the temperature, $D_a = D_0 e^{-E_a/kT}$ is the diffusion coefficient, with E_a being the activation energy. The boundary conditions (BCs) depend on wire topology.

When no current is applied, the stress in the wire is given by σ_T, the thermally-induced stress due to differentials in the coefficient of thermal expansion (CTE) in the materials that make up the interconnect stack. The differential equation with the boundary conditions can be solved numerically to obtain the transient behavior of stress over time. Due to superposition, the stress in the wire can be computed in this way and σ_T can then be added to account for CTE effects. The impact of σ_T is to offset the critical stress, σ_{crit}, to $(\sigma_{crit} - \sigma_T)$.

As in [10], the sign convention for j_i is in the direction of electron current, i.e., opposite to conventional current and the electric field. The atomic flux attributable to the electron wind force is proportional to the second term on the right hand side that contains j_i, while the flux related to the back-stress force is proportional to the first term containing the stress gradient $\frac{\partial \sigma}{\partial x}$. In both cases, the constant of proportionality varies linearly with the cross-sectional area of the wire. The sum, $(\partial \sigma/\partial x + \beta j_i)$, is proportional to the net atomic flux.

BCs for single-segment interconnect When electron current is injected through the anode and flows to the cathode at the other end, we have zero-flux conditions at each end:

$$\frac{\partial \sigma}{\partial x} + \beta j_1 = 0 \ \ \forall\, t \text{ at } x = 0, x = l_1. \quad (2)$$

BCs for a multisegment interconnect trees/meshes The boundary conditions at the terminus nodes (i.e., nodes of degree 1) require zero flux across the blocking boundary, i.e.,

$$\left.\frac{\partial \sigma_e}{\partial x}\right|_{\text{terminus}} + \beta j_e = 0 \quad (3)$$

where edge e connected to the terminus has current density j_e.

For any internal node n of the structure with degree $d \geq 2$, let the incident edges with reference current directed into the node be $\{e_1, \ldots, e_m\}$, and the edges directed away from the node be $\{e_{m+1}, \ldots, e_d\}$; if either set is empty, $m = 0$ or d. The flux boundary conditions at such a node are given by

$$\sum_{k \in \{1, \cdots, m\}} w_{e_k}\left(\left.\frac{\partial \sigma_{e_k}}{\partial x}\right|_n + \beta j_{e_k}\right) = \quad (4)$$

$$\sum_{k \in \{m+1, \cdots, d\}} w_{e_k}\left(\left.\frac{\partial \sigma_{e_k}}{\partial x}\right|_n + \beta j_{e_k}\right)$$

and the continuity boundary conditions are:

$$\sigma_{e_1}|_n = \sigma_{e_2}|_n = \cdots = \sigma_{e_d}|_n \quad (5)$$

where $\sigma_{e_k}|_n$ and $\partial \sigma_{e_k}/\partial x|_n$ are the values of the stress and its derivative at the location corresponding to node n.

III. ANALYSIS OF STEADY-STATE STRESS

A. Equations for steady-state analysis in a wire segment

We will work with (1) as a general representation of the stress in any multisegment line or tree. In the steady state, when the electron wind and back-stress forces reach equilibrium, then for each segment i, over its entire length, $0 \leq x \leq l_i$,

$$\frac{\partial \sigma_i}{\partial x} + \beta j_i = 0, \text{ i.e., } \frac{\partial \sigma_i}{\partial x} = -\beta j_i \quad (6)$$

The Blech criterion for immortality in a single-segment line states that in the steady state, if the maximum stress falls below the critical stress, σ_{crit}, required to nucleate a void, then the wire is considered immortal, i.e., immune to EM. This translates to the condition [1]:

$$jl \leq (jl)_{crit} \quad (7)$$

where $(jl)_{crit}$ is a function of the critical stress, σ_{crit}.

The derivation of the Blech criterion is predicated on the presence of blocking boundary conditions at either end of a segment carrying constant current, and is invalid for multisegment wires, even though it has been (mis)used in that context. For a general multisegment structure, from (6), *a linear gradient exists along each segment* of a general multisegment structure (this has been observed for multi-segment lines [12], [13] and meshes [16]).

Lemma 1: For edge e_k with reference current direction from vertex v_a to v_b, the steady-state stress along the segment is:

$$\sigma_k(x) = \sigma^a - \beta j_k x \quad (8)$$
$$\text{and } \sigma^b - \sigma^a = -\beta j_k l_k \quad (9)$$

where σ^a (σ^b) denotes the steady-state stress at node a (b).
Proof: The first expression follows directly from (6), and the second is obtained by substituting $x = l_k$ at node v_b. $\qquad\square$

The following corollary follows directly from (8):

Corollary 1: For edge $e_k = (v_a, v_b)$ in an interconnect structure,

$$\int_0^{l_k} \sigma_k(x)dx = \int_0^{l_k} (\sigma^a - \beta j_k x)dx = \sigma^a l_k - \beta j_k \frac{l_k^2}{2} \quad (10)$$

Corollary 2: In a segment, the largest stress is at an end point.
Proof: This follows from (9): if $j_k \geq 0$, the stress on the segment is maximized at node v_a; otherwise at node v_b. $\qquad \square$

B. Equations for steady-state analysis in a general structure

The existence of cycles in a graph requires careful consideration: we show that the solution can be found by analyzing a spanning tree.
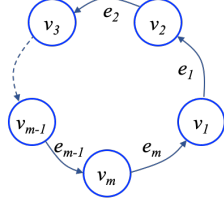

Figure 3: A cycle in $\mathcal{G}(V, E)$.

Theorem 1: Consider any undirected simple cycle, without repeated vertices or edges, $\mathcal{C}$ in $\mathcal{G}(V, E)$, consisting of edges $e_1, \cdots, e_m$ containing vertices $v_1, v_2, \cdots, v_m$, with edge reference directions from v_i to v_{i+1} (where $v_{m+1} \triangleq v_1$), as shown in Fig. 3. The m steady-state stress equations (9) representing this cycle are linearly dependent. A linearly independent set of equations is obtained by dropping one equation, i.e., breaking the cycle by dropping one edge.
Proof: Let V_i be the voltage at vertex v_i, R_i be the resistance of wire segment i, ρ be the wire resistivity, and h_i be the wire thickness (constant in layer i). Then $R_i = \rho l_i/(w_i h_i)$ and by Ohm's law,

$$j_i = (V_{i+1} - V_i)/(R_i w_i h_i) = (V_{i+1} - V_i)/(\rho l_i) \quad (11)$$

According to (9), along each edge $e_i = (v_i, v_{i+1})$,

$$\sigma^{i+1} - \sigma^i = -\beta j_i l_i = -\beta(V_{i+1} - V_i)/\rho \quad (12)$$

Adding up all equations (12) around the cycle, the left hand side sums up to zero, because each σ^k term in one equation has a corresponding $-\sigma^k$ term in the next equation (modulo m, so that $-\sigma^1$ and σ^1 appear in the last and first equation, respectively). Similarly, the right-hand side also sums up to zero due to telescopic cancelations of V^k in each equation and $-V^k$ in the next equation (modulo m).

Therefore, the m equations (12) are linearly dependent. They can be represented by $m - 1$ equations: by breaking the cycle at an arbitrary position and removing one edge, the simple cycle is transformed to a path with a set of independent linear equations. $\square$

The implications of Theorem 1 are profound, namely:
The steady-state stress in any structure with cycles can be solved by removing edges to make it acyclic, yielding a spanning tree structure, which is then solved to obtain the stress at all nodes.

C. Solving the steady-state analysis equations

We will first analyze a tree structure, since, as shown above, the steady state difference equations (9) are to be solved over a spanning tree of a general interconnect structure.

We choose an arbitrary leaf node of the tree as a reference; without loss of generality, we will refer to it as node v_1, and the stress at that node as σ^1. For any node v_i in the tree, there is a unique directed path $\mathcal{P}_i$ from v_1 to v_i, where each edge $e_k = (v_{s,k}, v_{t,k}) \in \mathcal{P}_i$ has a direction from $v_{s,k}$ to $v_{t,k}$ where $v_{s,k}$ is the vertex that is closer to v_1. Note that edges on this path are *directed* from v_1 towards v_i.
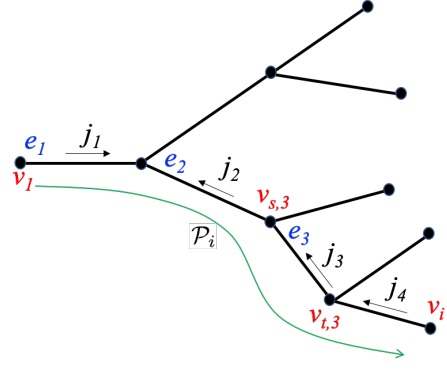

Figure 4: An example undirected graph of a tree-structured interconnect, showing path $\mathcal{P}_i$ from reference node v_1 to node v_i.

However, it is built on an *undirected* graph for the tree, where each undirected edge of the tree has a reference current direction.

To illustrate this point, consider the tree in Fig. 4, with path $\mathcal{P}_i$ from vertex v_1 to v_i. Vertex $v_{s,3}$ is the vertex of e_3 that is closer to v_1. The reference current directions on the undirected graph are as shown: the direction of j_1 is along the direction of path $\mathcal{P}_i$, while j_2, j_3, and j_4 are in the opposite direction.
Definition: We define $B_{\mathcal{P}_i}$, the "Blech sum" for a path $\mathcal{P}_i$, as:

$$B_{\mathcal{P}_i} = \sum_{e_k \in \mathcal{P}_i} \hat{j}_k l_k \quad (13)$$

where the summation is carried out over all edges e_k on path $\mathcal{P}_i$. The term $\hat{j}_k = j_k$ if the reference current direction for edge e_k is in the same as path $\mathcal{P}_i$; otherwise, $\hat{j}_k = -j_k$. Informally, $B_{\mathcal{P}_i}$ is the algebraic (jl) sum along $\mathcal{P}_i$ from v_1 to v_i.

In the example of Fig. 4, the Blech sum to $v_{s,3}$ is

$$B_{\mathcal{P}_{s,3}} = j_1 l_1 - j_2 l_2$$

Lemma 2: The stress, σ^i at node v_i is related to σ^1 as follows:

$$\sigma^i = \sigma^1 - \beta B_{\mathcal{P}_i} \quad (14)$$

Proof: In a tree, the path $\mathcal{P}_i$ must be unique [22]. Along this path, the current on each edge e_k from $v_{s,k}$ to $v_{t,k}$ is $\hat{j}_k$, i.e., j_k if the reference current direction is from $v_{s,k}$ to $v_{t,k}$, and $-j_k$ otherwise. Therefore, from (9),

$$\sigma^{t,k} - \sigma^{s,k} = -\beta \hat{j}_k l_k \quad (15)$$

The continuity boundary condition (5) ensures that the stress at the distal end of an edge on $\mathcal{P}_i$ is identical to that on the proximal end of its succeeding edge, i.e., for successive edges e_k and e_l on $\mathcal{P}_i$, $\sigma^{t,k} = \sigma^{s,l}$. Therefore, adding these equations over all edges on path $\mathcal{P}_k$, we see that as successive edges on the path share a vertex v, σ^v cancels out telescopically, except for $v = v_1$ or v_i. Meanwhile, the $\beta \hat{j}_k l_k$ terms add up, so that the sum of all equations yields

$$\sigma^i - \sigma^1 = -\beta \sum_{e_k \in \mathcal{P}_i} \hat{j}_k l_k \quad (16)$$

This leads to the result in (14). $\qquad \square$

However, (14) in Lemma 2 stops short of determining σ^i at each node: for a tree with $|V|$ nodes, the lemma provides $(|V| - 1)$ linear equations in $|V|$ variables, leading to an underdetermined system where each node stress is related to the stress, σ^1, at an arbitrarily chosen leaf node, n_1. The $|V|^{\text{th}}$ equation is obtained from the principle of the conservation of mass: atoms are transported along a wire, but with zero net change in the number of atoms in the wire.

3

Lemma 3: For a general tree/mesh interconnect with $|E|$ edges, with edge k having width w_k and height h_k,

$$\sum_{k=1}^{|E|} w_k h_k \int_0^{l_k} \sigma_k(x) dx = 0 \quad (17)$$

The proof of the lemma is in the appendix and generalizes a similar result from [16]. In effect, this is an integral form of the BCs (4), which conserve flux at the boundary of each segment in the tree.

Theorem 2: A tree or mesh interconnect with $|E|$ edges and $|V|$ vertices is immortal when:

$$\max_{1 \le i \le |V|} \left(\sigma^i \right) < \sigma_{crit} \quad (18)$$

where $\sigma^i = \beta \left[\dfrac{\sum_{k=1}^{|E|} w_k h_k \left[\hat{j}_k \frac{l_k^2}{2} - B_{\mathcal{P}_{s,k}} l_k \right]}{\sum_{k=1}^{|E|} w_k h_k l_k} - B_{\mathcal{P}_i} \right]$ (19)

where $B_{\mathcal{P}_i}$ is the "Blech sum" defined in (13).

Proof: We first show that expression (19) provides the stress at node n_i of the interconnect, and is obtained by combining the result of Lemma 3 with the $(|V| - 1)$ equations from (14).

Let edge e_k connect vertices $v_{s,k}$ and $v_{t,k}$, where $v_{s,k}$ is the vertex that is closer in the tree to the reference node v_1. Then, substituting the result of Lemma 2 into Corollary 1,

$$\int_0^{l_k} \sigma(x) dx = \left(\sigma^1 - \beta B_{\mathcal{P}_{s,k}} \right) l_k - \beta \hat{j}_k \frac{l_k^2}{2} \quad (20)$$

where $B_{\mathcal{P}_{s,k}}$ is the Blech sum from node n_1 to node $v_{s,k}$.[1]

Substituting the integral expressions in (17) from Lemma 3:

$$\sum_{k=1}^{|E|} w_k h_k \left[\left(\sigma^1 - \beta B_{\mathcal{P}_{s,k}} \right) l_k - \beta \hat{j}_k \frac{l_k^2}{2} \right] = 0 \quad (21)$$

After further algebraic manipulations, we obtain

$$\sigma^1 = \frac{\beta \sum_{k=1}^{|E|} w_k h_k \left[\hat{j}_k \frac{l_k^2}{2} + B_{\mathcal{P}_{s,k}} l_k \right]}{\sum_{k=1}^{|E|} w_k h_k l_k} \quad (22)$$

Finally, we substitute the above into (14) to obtain (19), the expression for the steady-state stress values at each node i.

For the interconnect to be immortal, the largest value of stress in the tree must be lower than σ_{crit}, the critical stress required to induce a void. From Corollary 2, in finding the maximum stress in the tree, it is sufficient to examine the stress at the nodes of the tree, so that the largest node stress is below σ_{crit}. This proves (18). $\square$

IV. Linear-Time Immortality Calculation

As we have established, a general interconnect on a graph can be solved by considering the solution of Theorem 1 on a tree of the graph. Identifying such tree is straightforward, and standard methods such as depth-first or breadth-first traversal can be used.

After arriving at a tree structure, although Theorem 2 provides a useful, closed-form result, a simple-minded computation would calculate σ^i at each node v_i in the tree through repeated incantations of (19). However, as we will show, this computation can be performed in $O(|E|)$ time for a structure with $|E|$ edges. We rewrite (19) as:

$$\sigma^i = \beta \left[\frac{Q}{A} - B_{\mathcal{P}_i} \right] \quad (23)$$

where $Q = \sum_{k=1}^{|E|} w_k h_k \left[\hat{j}_k \frac{l_k^2}{2} + B_{\mathcal{P}_{s,k}} l_k \right]$ (24)

$$A = \sum_{k=1}^{|E|} w_k h_k l_k \quad (25)$$

---

[1]The use of $\hat{j}_k$ allows for the traversal from v_1 to v_i to include edges in a direction opposite to the reference current direction: the stress difference between nodes on such edges should have the opposite sign as (9) in Lemma 1.

This computation requires the calculation of three summations for A, Q, and for the Blech sum, $B_{\mathcal{P}_i}$ from reference node v_1 to each node i in the tree. It proceeds in the following steps:

1. To compute $B_{\mathcal{P}_i}$, we traverse the tree from v_1 using a standard traversal method, e.g., the breadth-first search (BFS). At node v_1, we initialize $B_{\mathcal{P}_{v_1}} = 0$. As we traverse each edge $e_k = (v_{s,k}, v_{t,k})$, we compute $B_{\mathcal{P}_{t,k}}$.
2. Using the above Blech sums to each node, we compute Q (Eq. (24)) and A (Eq. (25)), summing over all edges.
3. Finally, we compute σ^i at each node i using (23).

Complexity analysis: The BFS traversal in Step 1 over a tree traverses $O(|E|)$ edges. For each edge, Step 2 performs a constant number of computations to obtain A and Q ((25)–(24)). The final computation of (23) in Step 3, and the immortality check that compares the computed value with $(\sigma_{crit} - \sigma_T)$ according to (18), perform a constant number of computations for $|V|$ nodes. Therefore, the computational complexity for any tree structure is $O(|E|)$.
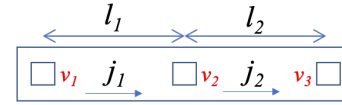

Figure 5: A two-segment interconnect line.

Example: We illustrate our computation for a two-segment line (Fig. 5) in a single layer (with constant h_k) in Table I, using the leftmost node v_1 as the reference. Starting from v_1, the two edges are traversed to compute B. The symbol $B_{\mathcal{P}_{t,k}}$ represents the Blech sum calculated at the distal vertex $v_{t,k}$ of the edge; note that the computation of Q uses the Blech sum at the proximal vertex, $v_{s,k}$.

Table I: Sequence of computations for a two-segment wire.

	A	$B_{\mathcal{P}_{t,k}}$	Q
Initializaton	0	0	0
Edge (v_1, v_2)	$w_1 l_1$	$j_1 l_1$	$w_1 j_1 l_1^2 / 2$
Edge (v_2, v_3)	$w_1 l_1 + w_2 l_2$	$j_1 l_1 + j_2 l_2$	$w_1 j_1 l_1^2/2 + w_2 j_2 l_2^2/2$ $+ w_2 l_2 (j_1 l_1)$

Based on the table, we compute the stress at each node as:

$$\sigma^{v_1} = \beta \frac{w_1 j_1 l_1^2 + w_2 j_2 l_2^2 + 2 w_2 j_1 l_1 l_2}{2(w_1 l_1 + w_2 l_2)} \quad (26)$$

$$\sigma^{v_2} = \sigma^{v_1} - \beta(j_1 l_1) \; ; \; \sigma^{v_3} = \sigma^{v_1} - \beta(j_1 l_1 + j_2 l_2)$$

The analysis of this line in [19] yields an identical result; unlike our method, [19] cannot analyze arbitrary trees/meshes in linear time.

V. Results

We present three sets of results. The first set shows comparisons with a numerical solver in Section V-A. Next, in Section V-B, we use our method to analyze large public-domain IBM power grid benchmarks. These were designed for old Al lines, but we assume them to be modern Cu DD wires. The large sizes of these benchmarks test the scalability of our approach. Finally, in Section V-C, we perform analysis of power grids on designs synthesized on a commercial 28nm and Nangate 45nm parameters, both based on Cu DD interconnects.

In Cu DD based technologies, each layer can be treated separately due to the presence of barrier/capping layers that prevent atomic flux from flowing across layers through vias. The methods in this paper are applied to each layer to find the steady-state stress, which is then used to predict immortality. This limits the size of the EM problem, since it must be solved in a single layer at a time. Moreover, since it is common to use a reserved layer model where all wires in a layer are in the same direction, effectively this implies that each layer consists of a set of metal lines with a limited number of nodes. In
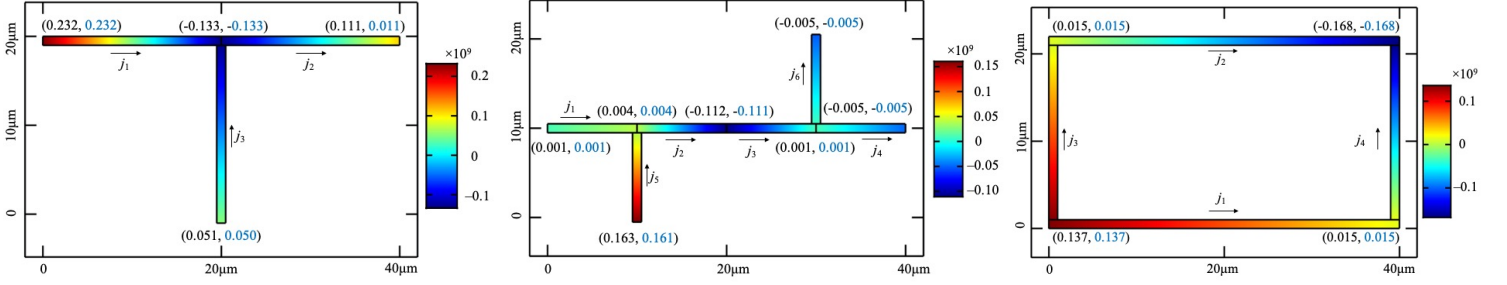
Figure 6: Comparison of the steady-state stress in three structures: a T, a tree, and a mesh. The stress at each node (in GPa) is shown as a tuple, with our closed-form solution in black and the COMSOL solution in blue text. The color bar is based on a COMSOL solution. The width of each segment is $1\mu m$, and length scales are shown in the figure. The current densities in the T are $j_1 = 6 \times 10^{10} A/m^2$, $j_2 = -4 \times 10^{10} A/m^2$, $j_3 = 3 \times 10^{10} A/m^2$. For the tree, $j_1 = -1 \times 10^{10} A/m^2$, $j_2 = 5 \times 10^{10} A/m^2$, $j_3 = -4 \times 10^{10} A/m^2$, $j_4 = j_6 = 2 \times 10^{10} A/m^2$, $j_5 = 4 \times 10^{10} A/m^2$. For the mesh structure, $j_1 = 1 \times 10^{10} A/m^2$, $j_2 = 1.5 \times 10^{10} A/m^2$, $j_3 = 2 \times 10^{10} A/m^2$, $j_4 = 3 \times 10^{10} A/m^2$.

such scenarios, the EM problem reduces to the analysis of a large number of line/tree structures, each with tens of nodes. The IBM benchmarks contain mesh structures within layers, which enable us to better evaluate our method.

A. Comparison with COMSOL

We show comparisons between our approach and numerical simulations using COMSOL on Cu DD based structures. The material parameters, provided to COMSOL, are [14]: $\rho = 2.25e\text{-}8\Omega m$, $\mathcal{B} = 28\text{GPa}$, $\Omega = 1.18e\text{-}29m^3$, $D_0 = 1.3e\text{-}9m^2/s$, $E_a = 0.8eV$, $Z^* = 1$, $\sigma_{crit} = 41\text{MPa}$, $T = 378\text{K}$. COMSOL is limited to analyzing small structures, which is reflected the topologies shown in Fig. 6:

- An interconnect tree with three segments
- A larger interconnect tree
- A simple mesh structure

The color maps in the figure show the spatial variation of steady-state stress over each interconnect, where the numbers next to each node represent the values computed using our approach and by COMSOL. It is easily seen that the numbers match; since our approach is exact, any discrepancies can be attributed to numerical inaccuracies in COMSOL.

B. Analysis on IBM power grid benchmarks

The only widely available power grid benchmarks are the IBM benchmarks [23]. Each benchmark contains Vdd and Vss networks and multiple voltage domains, and general tree/mesh structures in individual layers. We implement a BFS traversal over these structures using Python3.6 and Deep Graph Library [24] on a GPU by modifying the message passing functions. Run times are shown on a 3.6GHz Intel Core i7-7820X and NVIDIA RTX 2080Ti GPU.
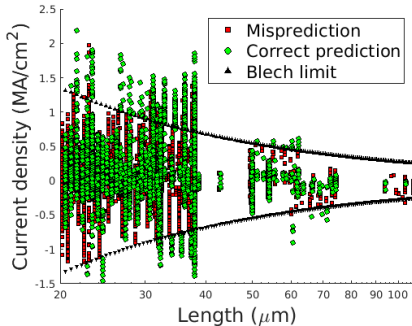

Figure 7: Inaccuracy of the traditional Blech filter (ibmpg6).

The traditional Blech criterion is only accurate for a single-segment wire: next, we evaluate its accuracy. We consider our approach

Table II: Comparison of our approach against the traditional Blech filter on the IBM benchmarks (TP = true positive, TN = true negative, FP = false positive, FN = false negative.)

	$|E|$	TP	TN	**FP**	**FN**	Runtime	
						GPU	CPU
pg1	29750	1557	10144	**17372**	**677**	7s	6s
pg2	125668	7703	33534	**82025**	**2406**	12s	19s
pg3	835071	200158	3539	**630979**	**395**	36s	184s
pg6	1648621	916094	1365	**730995**	**167**	88s	280s

as the accurate result since it is rigorously derived for multisegment structures by generalizing the same physics-based modeling framework used by the Blech criterion for one-segment wires, and it is validated on COMSOL. Therefore a positive identification of immortality implies that our method finds the segment to be immortal; a negative identification implies mortality.

Fig. 7 plots the current density j vs. the wire length l within the segments of the ibmpg6 benchmark. The currents in the Vdd and Vss lines may be either positive or negative, and their magnitude affects EM. The black triangles show the contours of $jl = (jl)_{crit}$: when the magnitude lies within this frontier for a segment of the grid, the traditional Blech criterion (7) would label the wire as immortal; otherwise it is potentially mortal. To help highlight erroneous predictions, the figure shows green markers for correct predictions and red markers for incorrect predictions. The Blech criterion shows significant inaccuracy on multisegment wires.

Table II summarizes the results on IBM benchmarks. True positives (TP) and true negatives (TN) correspond to correct predictions where the Blech criterion agrees with our accurate analysis. The errors correspond to *false negatives* (FN), where an immortal segment is deemed potentially mortal by the traditional Blech criterion, and *false positives* (FP), where an mortal segment is labeled as potentially immortal by Blech. FPs cause failures to be overlooked, and FNs may lead to overdesign as EM-immortal wires are needlessly optimized.

The table shows that:

- the inaccuracies in the Blech filter are seen across benchmarks.
- our method is scalable to large mesh sizes with low runtimes.

From the data, it is apparent that the traditional Blech criterion can provide misleading results. The reasons for this are twofold:

- A high-jl segment could be immortal if it has numerous downstream segments with low jl, so that the total jl sum may be low. For example, in Fig. 5, if the current density $j_1 = 0$, then the segment acts as passive reservoir, bringing down the stress in the right segment to be lower than the case of an identical isolated segment carrying the same current, but with a blocking boundary at v_2 [18].

Table III: Comparison of our approach against the traditional Blech filter on a 28nm technology with Cu interconnects.

	Circuit	$|E|$	TP	TN	**FP**	**FN**
	gcd	678	634	8	**31**	**5**
28nm	aes	11,361	8,039	0	**3,297**	**25**
	jpeg	123,220	63,889	71	**58,696**	**564**
	dynamic_node	6,270	2,617	256	**3,059**	**338**
	aes	7,212	3,255	322	**3,160**	**475**
45nm	ibex	12,128	4,645	1,112	**4,964**	**1,407**
	jpeg	35,848	10,052	5,047	**15,479**	**5,270**
	swerv	59,049	14,545	9,762	**23,366**	**11,376**

- A low-jl segment could be labeled immortal by the traditional criterion, but it may be mortal due to a high stress at one node, caused by a high Blech sum for downstream wire segments, which could raise the stress at the other node.

C. Analysis on OpenROAD power grids

We show simulations based on power grids from circuits designed using a commercial 28nm and Nangate45 technologies using Cu DD interconnects. The circuits are taken through synthesis, placement and routing in these technology nodes (some circuits are implemented in both nodes) using a standard design flow. The power grid is synthesized using an open-source tool, OpeNPDN [25] from OpenROAD. The IR drop and currents are computed using PDNSim [26], with currents scaled to provide an IR drop of 5mV.

Fig. 8 shows a scatter plot that analyzes the inaccuracy of the traditional Blech criterion on a Cu-based technology, using $(jl)_{crit} = 0.27$A/μm, based on material parameters listed in Section V-A. Due to the regular structure of the power grid, many lines have the same length. As in the earlier case, it is easily seen that the Blech criterion leads to numerous false positives and false negatives. Results for more circuits are listed in Table III, and show similar trends.
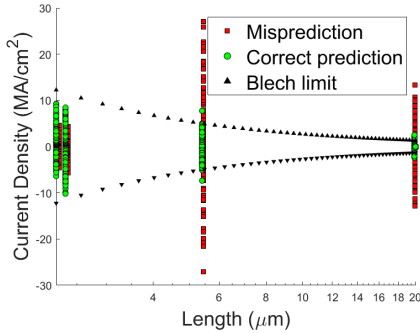

Figure 8: Inaccuracy of traditional Blech filter (jpeg/28nm).

VI. Conclusion

A linear-time approach for checking immortality in a general tree/mesh interconnect is proposed. The results are validated against COMSOL and shown to be fast and scalable to large power grids.

Appendix: Proof of Lemma 3

Proof: The stress on a wire segment causes a displacement of u_i in segment i of the interconnect structure. The stress has no shear component since the current in a line is unidirectional. Due to conservation of mass, the net material coming from all $|E|$ wire segments is zero, and therefore,

$$\sum_{k=1}^{|E|} w_k h_k u_k = 0 \qquad (27)$$

where w_k is the width of the kth wire segment. The displacement u_k is the integral of displacements du_k over the segment caused by

stress $\sigma_k(x)$ applied on elements of size dx in segment k. If $\mathcal{B}$ is the bulk modulus, from Hooke's law,

$$u_k = \int_0^{l_k} du_k(x) = \mathcal{B} \int_0^{l_k} \sigma_k(x)dx \qquad (28)$$

Combining this with (27) leads to the result of Lemma 3. $\qquad\square$

References

[1] I. A. Blech, "Electromigration in thin aluminum films on titanium nitride," *J. Appl. Phys.*, vol. 47, no. 4, pp. 1203–1208, 1976.

[2] J. R. Black, "Electromigration failure modes in aluminum metallization for semiconductor devices," *Proc. IEEE*, vol. 57, no. 9, pp. 1587–1594, 1969.

[3] H.-B. Chen, *et al.*, "Analytical modeling and characterization of electromigration effects for multibranch interconnect trees," *IEEE T. Comput. Aid D.*, vol. 35, no. 11, pp. 1811–1824, 2016.

[4] S. Chatterjee, *et al.*, "Power grid electromigration checking using physics-based models," *IEEE T. Comput. Aid D.*, vol. 37, pp. 1317–1330, July 2018.

[5] V. Mishra and S. S. Sapatnekar, "The impact of electromigration in copper interconnects on power grid integrity," in *Proc. DAC*, pp. 88:1–88:6, 2013.

[6] V. Mishra and S. S. Sapatnekar, "Predicting electromigration mortality under temperature and product lifetime specifications," in *Proc. DAC*, pp. 43:1–43:6, 2016.

[7] R. Rosenberg and M. Ohring, "Void formation and growth during electromigration in thin films," *J. Appl. Phys.*, vol. 42, no. 13, pp. 5671–5679, 1971.

[8] M. Schatzkes and J. R. Lloyd, "A model for conductor failure considering diffusion concurrently with electromigration resulting in a current exponent of 2," *J. Appl. Phys.*, vol. 59, pp. 3890–3893, 1986.

[9] J. J. Clement and J. R. Lloyd, "Numerical investigations of the electromigration boundary value problem," *J. Appl. Phys.*, vol. 71, pp. 1729–1731, 1992.

[10] M. A. Korhonen, *et al.*, "Stress evolution due to electromigration in confined metal lines," *J. Appl. Phys.*, vol. 73, no. 8, pp. 3790–3799, 1993.

[11] V. Sukharev, "Beyond Black's equation: Full-chip EM/SM assessment in 3D IC stack," *Microelectronic Engineering*, vol. 120, pp. 99–105, 2014.

[12] S. P. Riege, *et al.*, "A hierarchical reliability analysis for circuit design evaluation," *IEEE T. Electron Dev.*, vol. 45, pp. 2254–2257, Oct. 1998.

[13] J. J. Clement, *et al.*, "Methodology for electromigration critical threshold design rule evaluation," *IEEE T. Comput. Aid D.*, vol. 18, pp. 576–581, May 1999.

[14] S. M. Alam, *et al.*, "Circuit-level reliability requirements for Cu metallization," *IEEE T. Device Mater. Rel.*, vol. 5, no. 3, pp. 522–531, 2005.

[15] A. Abbasinasab and M. Marek-Sadowska, "Blech effect in interconnects: Applications and design guidelines," in *Proc. ISPD*, pp. 111–118, 2015.

[16] H. Haznedar, *et al.*, "Impact of stress-induced backflow on full-chip electromigration risk assessment," *IEEE T. Comput. Aid D.*, vol. 25, pp. 1038–1046, June 2006.

[17] M. H. Lin and A. S. Oates, "An electromigration failure distribution model for short-length conductors incorporating passive sinks/reservoirs," *IEEE T. Device Mater. Rel.*, vol. 13, pp. 322–326, Mar. 2013.

[18] M. H. Lin and A. S. Oates, "Electromigration failure of circuit interconnects," in *Proc. IRPS*, pp. 5B–2–1–5B–2–8, 2016.

[19] Z. Sun, *et al.*, "Fast electromigration immortality analysis for multisegment copper interconnect wires," *IEEE T. Comput. Aid D.*, vol. 37, pp. 3137–3150, Dec. 2018.

[20] J. Gambino, "Process technology for copper interconnects," in *Handbook of Thin Film Deposition* (K. Seshan and D. Schepis, eds.), ch. 6, pp. 147–194, Amsterdam, The Netherlands: Elsevier, 3rd ed., 2018.

[21] L. Zhang, *et al.*, "Grain size and cap layer effects on electromigration reliability of cu interconnects: Experiments and simulation," in *AIP Conf. Proc.*, vol. 1300, 3, 2010.

[22] T. H. Cormen, *et al.*, *Introduction to Algorithms*. Boston, MA: MIT Press, 3rd ed., 2009.

[23] "IBM power grid benchmarks." https://web.ece.ucsb.edu/~lip/PGBenchmarks/ibmpgbench.html, Accessed April 6, 2021.

[24] M. Wang, *et al.*, "Deep graph library: A graph-centric, highly-performant package for graph neural networks," in *arXiv:1909.01315 [cs.ar]*, 2020.

[25] V. A. Chhabria, *et al.*, "Template-based PDN synthesis in floorplan and placement using classifier and CNN techniques," in *Proc. ASP-DAC*, pp. 44–49, 2020.

[26] "PDNSim." github.com/The-OpenROAD-Project/OpenROAD/tree/master/src/PDNSim. Accessed April 6, 2021.